Biosensors and Bioelectronics 66 (2015) 474–480

Contents lists available at ScienceDirect

Biosensors and Bioelectronics

journal homepage: www.elsevier.com/locate/bios

Au nanoparticle/graphene nanocomposite as a platform for the sensitive detection of NADH in human urine

Maduraiveeran Govindhan, Mona Amiri, Aicheng Chen *

Department of Chemistry, Lakehead University, 955 Oliver Road, Thunder Bay, ON, Canada P7B 5E1

ARTICLE INFO

Article history:
Received 30 September 2014
Received in revised form
1 December 2014
Accepted 2 December 2014
Available online 3 December 2014

Keywords:
Au nanoparticle
Graphene
Modified electrode
Electrocatalysis
Biosensor
NADH

ABSTRACT

Here we report on a facile, rapid, sensitive, selective and highly stable electrochemical sensing platform for β-nicotinamide adenine dinucleotide (NADH) based on uncapped Au nanoparticle/reduced graphene oxide (rGO) nanocomposites without the aid of any redox mediators and enzymes. The Au nanoparticle/rGO composite sensing platform was directly formed on a glassy carbon electrode through an in situ electrochemical reduction of GO and Au^{3+} with a 100% usage of the precursors. The as-prepared Au nanoparticle/rGO composites demonstrated excellent direct electrocatalytic oxidation toward NADH, providing a large electrochemical active surface area as well as a favorable environment for electron transfer from NADH to the electrode via the enhanced mobility of charge carriers. The Au nanoparticle/rGO composites offered a ~2.3 times higher electrocatalytic current density with a negative shift of 112 mV, in comparison to Au nanoparticles. The sensor developed in this study displayed a high sensitivity of 0.916 μA/μM cm^2 and a wide linear range of from 50 nM to 500 μM with a limit of detection of 1.13 nM (S/N=3). The interferences from the common interferents such as glutathione, glucose, ascorbic acid and quanine were negligible. The prepared sensor was further tested for the determination of NADH in human urine samples, showing the Au nanoparticle/rGO nanocomposites simultaneously formed by one-step electrochemical reduction have promising biomedical applications.

1. Introduction

NADH/NAD^+ is a vital co-enzyme couple that plays a significant role in energy production/consumption within the cells of living organisms, which participates in a variety of enzymatic reactions involving more than 300 dehydrogenases (Ali et al., 2014; Bergel and Comtat, 1989). From fundamental science to practical technological applications, many research studies have been focused on the NADH reaction, including electrochemical investigation (Moradi et al., 2013; Wu et al., 2007). Some researchers have found that NADH is beneficial for patients who are suffering from Parkinson's disease, Alzheimer's disease, and depression (Lin and Guarente, 2003; Moradi et al., 2013). Studies have also shown that NADH is required for the regeneration of glutathione (GSH) following its oxidation. GSH levels may also fall immediately should NADH levels be depleted. Therefore, supplementation with NADH might also facilitate the restoration of GSH to its active form (Serban and Murr, 2004). NADH is also crucial as a co-factor of other enzymes in biological, clinical and pharmaceutical samples (Limoges et al., 2006; Wei et al., 2008). Due to its importance in dehydrogenase-based bioelectrochemical devices, such as biosensors, biofuel cells, and bioreactors, NADH detection has received much attention (Radoi and Compagnone, 2009). However, the direct oxidation of NADH at conventional solid electrodes is highly irreversible, requiring considerable activation energy, and proceeds with coupled side reactions, which poison the electrode surface via side products such as methyl, propyl and benzyl reactants that strongly adsorb onto the electrode surface (Ali and Omanovic, 2014; Deore and Freund, 2005). A variety of analytical methods have been proposed for NADH sensing, including colorimetry (Liu et al., 2012), photoelectrochemistry (Li et al., 2014; Wang et al., 2009), enzymatic assay (Ricci et al., 2007), and high-performance liquid chromatography (Downey and Nieman, 1992). Among these methods, electrochemical sensors are likely to offer a highly sensitive analytical approach for the detection of NADH, due to their rapid response, straightforward operation, and cost effectiveness (Chen and Shah, 2013; Lin et al., 2007).

Currently, much effort is being invested in research into new materials toward the development of the electrochemical biosensors with sensitive and rapid response (Kimmel et al., 2012). Electrochemical biosensors are attractive for analytical applications due to their unique specificity (Chatterjee et al., 2013), and the development of composite electrodes may lead to further improvement in biosensing devices. Over the past two decades,

* Corresponding author. Fax: +1 807 346 7775.
E-mail address: aicheng.chen@lakeheadu.ca (A. Chen).

http://dx.doi.org/10.1016/j.bios.2014.12.012
0956-5663/

the development of rapid, robust, sensitive, selective, and cost effective sensors with low detection limits have been a primary interest in the bioanalytical sciences (Chen and Chatterjee, 2013). Amperometric sensors offer high sensitivity with a wide linear range, which comprise the most commonly used chemo- and biosensors (Turner, 1988). Amperometric detection is particularly important in bioanalytical devices as relates to the detection of low concentrations of specific biomarkers, such as NADH (Lin et al., 2014), cysteine (Dalkiran et al., 2014) and glucose (Wang et al., 2008). Biomarkers participate in cellular metabolic redox reactions to assist in the regulation of biological activities (Chikkaveeraiah et al., 2012).

Recently, many nanomaterials have been designed and employed as the electrocatalysts, including carbon based nanomaterials for NADH oxidation without the aid of redox mediators (Li et al., 2014). Graphene, which consists of a two dimensional single layer of sp^2-hybridized carbon atoms, has attracted a great deal of attention from both experimental and theoretical scientific communities (Bolotin, 2014; Qian et al., 2011a,b). In addition, recent studies have demonstrated that graphene is a promising candidate for use as an advanced carbon based material in the electrochemical applications (Chen et al., 2012; Liu et al., 2014; Qian et al., 2011a,b). The combination of attributes such as high surface area, enhanced mobility of charge carriers, and high stability makes graphene an ideal platform for the anchoring of metal particles in electrochemical sensing applications (Liu et al., 2013; Vedala et al., 2011; Liu et al., 2014). Most recently, Lin and co-workers (Lin et al., 2014) have demonstrated the detection of NADH utilizing graphene oxide (GO) and multi-walled carbon nanotube (GO-MWCNT) composites. Au nanoparticles, with their inherent biocompatibility, ease of preparation, and high stability, have been used widely as immobilization matrices for electrochemical biosensors (Saha et al., 2012) and bioelectrocatalysis (Pelaz and Pino, 2012). In particular, Au nanoparticle supported graphene has the capacity for robust catalytic performance toward biomolecules due to an increase in charge transfer, from the nanoparticles to the substrates. The stability of the system might also be improved via hybridization between the nanoparticles and sp^2 dangling bonds at graphene resident defect sites (Artiles et al., 2011; Liu et al., 2014).

In the present work, we report on a novel nanocomposite of Au nanoparticles and reduced GO (rGO), which was directly formed on a glassy carbon electrode (GCE) by one-step electrochemical reduction of GO and Au precursors, for the sensitive detection of NADH. The significant advantages of this innovative method includes (i) a facile and rapid electrochemical synthetic strategy; (ii) forming highly dense and uniform Au nanoparticles/rGO nanocomposite in the absence of any capping agents; (iii) cost effectiveness with a 100% usage of precursors, and (iv) a green approach where no organic solvents and harzardous reducing agents were used. The as-prepared Au nanoparticle/rGO composite modified GCE (designated as Au–rGO/GCE) exhibited high electrocatalytic activity and stability for NADH oxidation without any further surface modification, and showed an excellent performance for the sensitive detection of NADH.

2. Experimental

2.1. Materials

GO, Au chloride, and a 10 wt% Nafion solution were obtained from Sigma-Aldrich. NADH, glucose, guanine, ascorbic acid and glutathione were supplied by Sigma-Aldrich. All other analytical grade reagents were used as received. All electrochemical experiments were performed in a 0.1 M H_2SO_4 electrolyte and a phosphate buffer solution (PBS). Pure water (18.2 MΩ cm), purified with a Nanopure® water system, was used in the preparation of all solutions. A 10.0 mM NADH stock solution was prepared daily by dissolving NADH in water, followed by refrigeration at 4 °C in the dark.

2.2. Characterization and electrochemical measurements

Surface morphology and composition were characterized using a field-emission scanning electron microscopy (FE-SEM) and energy-dispersive X-ray spectroscopy (EDX) (Hitachi SU-70). X-ray diffraction patterns of the formed rGO and the Au nanoparticles/rGO nanocomposite were recorded with a Pananalytical Xpert Pro Diffractometer with Ni filtered monochromatic Cu Kr (1.5406 Å, 2.2 kW max.). ThermoFisher X-ray photoelectron spectroscopy (XPS) was employed to study the composition as well as the oxidation states of the formed Au nanoparticles/rGO thin film, where the size of the X-ray spot was 400 μm with an Al Kα monochromatic source.

Electrochemical experiments were conducted using a CHI 660B electrochemical workstation (CH Instrument Inc. USA) employing a conventional one-compartment three-electrode cell system. A GCE was utilized as the working electrode substrate with a geometric surface area of 0.07 cm^2; whereas a silver/silver chloride electrode (Ag/AgCl) served as the reference electrode, and a platinum coil was used as the counter electrode. Ar was used to purge the solution to achieve an O_2-free condition. All of the electrochemical experiments were performed at room temperature, 20 ± 2 °C.

2.3. Preparation of samples

Human urine samples were refrigerated immediately following collection from a volunteer. A known volume (5 mL) of the sample was centrifuged for 10 min at 12,000 rpm (Sorvall Biofuge Stratos Centrifuge, Thermo Electron Corporation). The supernatant was filtered and then diluted 10 times with 0.1 M PBS (pH 7.2). The solution was transferred into the electrochemical cell for analysis without any further pretreatment. A stock solution of 1.0 mM NADH was prepared and stored in the refrigerator, which was further diluted to obtain 10.0, 20.0 and 30.0 μM NADH. The amperometric *i–t* measurements were carried out for the recovery tests to determine NADH in the human urine samples.

2.4. Fabrication of the electrochemical sensor

The Au–rGO/GCE was fabricated by in situ electrochemical reduction of the GO and Au precursors (Govindhan and Chen 2015). The GCE was double polished using alumina powder (0.05 μm) followed by sonication in the pure water for 3 min. A known amount of 5 μL mixture of GO (0.5 mg/mL), $AuCl_3$ (10 mM) and Nafion (0.5%), was cast on the cleaned GC electrode and then allowed to air dry. The in situ formation of Au nanoparticle/rGO sheets on the GCE was accomplished in 0.1 M H_2SO_4 by applying a potential of −1.0 V (vs Ag/AgCl) for 125, 250, 500 and 750 s. For comparison, Au nanoparticles as well as rGO sheets were formed on the GCE surface (termed as Au/GCE and rGO/GCE, respectively) using the same electrochemical reduction approach under the similar experimental conditions, where the electrochemical reduction time was set for 500 s. The prepared electrodes were stored in the pure water for further electrochemical measurements.

3. Results and discussion

3.1. Characterization of Au nanoparticle/rGO nanocomposites

Fig. 1A displays a FE-SEM image of the rGO sheets, where the insets show the photographs of the GO film before and after the electrochemical reduction. A substantial color change was observed; the GO film was altered from a light yellow color (inset i) to a black color (inset ii) subsequent to the electrochemical reduction of GO, indicating the formation of the reduced GO (rGO). A typical FE-SEM image of the Au nanoparticles/rGO nanocomposite produced after the 500-s electrochemical reduction is presented in Fig. 1B, showing that the Au nanoparticles with an average particle size of 8.2 nm were uniformly distributed on the rGO sheet. As seen in the inset photographs of Fig. 1B, the greenish yellow Au precursors/GO coating (inset i) was changed to the shadowy brown Au nanoparticle/rGO film (inset ii). EDX analysis (Fig. 1C) further confirmed the coexistence of the formed Au/rGO thin film. Fig. 1D displays the XRD patterns of the synthesized rGO sheets (blue) and the Au nanoparticle/rGO nanocomposite (red). The appearance of the (002) peak at 25.4° indicated that the formed rGO via the electrochemical reduction of GO exhibited the crystalline nature of graphene (Xu and Gao, 2011). The (111), (200), (220) and (311) planes corresponded to a face centered Au cubic lattice. All these results show that the electrochemical approach used in this study is efficient for the in situ simultaneously reduction of Au^{3+} and GO to form the uniform Au nanoparticle/rGO nanocomposite on the electrode surface. The crystalline size for the Au nanoparticles was estimated to be 9.3 nm using Scherrer's equation (Cullity, 1978), which is consistent with the SEM observation.

To further confirm the formation of rGO and the Au nanoparticles, XPS analysis was conducted for the GO, rGO and Au nanoparticle/rGO composite samples. The high-resolution C1s spectra of GO and rGO are presented in Fig. 2A and B, respectively. Four fitting peaks were observed at 284.6, 286.3, 287.4 and 288.5 eV, corresponding to sp^2 C, C–OH, C=O and HO–C=O, respectively (Wagner et al., 1979). As seen in Table S1, a significant decrease of the atomic percentage of C–OH, C=O, and HO–C=O was observed for rGO when compared to GO, showing the effective removal of oxygen functional groups from the surface of GO by the electrochemical reduction. Fig. 2C displays the XPS doublet peak at 84.6 eV ($Au4f_{7/2}$) and 88.3 eV ($Au4f_{5/2}$) for Au^0 (Luo et al., 2012) and the percentage of the metallic state of Au was calculated from the 4f XPS analysis. It was found that almost 100% of Au was in its metallic state, demonstrating that the successful reduction of the Au precursor to form Au nanoparticles on the rGO sheets by the facile electrochemical method.

Fig. 3A presents the cyclic voltammograms of the Au/GCE (pink) and Au–rGO/GCE (red) recorded in 0.1 M H_2SO_4 at 20 mV s^{-1}, where typical oxide formation and reduction of Au nanoparticles were observed (Maduraiveeran and Ramaraj, 2007). The oxidation peak of the Au–rGO/GCE appeared at 0.95 V, with a corresponding reduction peak at 0.49 V; whereas the oxidation peak of the Au/GCE appeared at 0.91 V, with a corresponding reduction peak at 0.45 V. Besides the shift of the both oxidation and

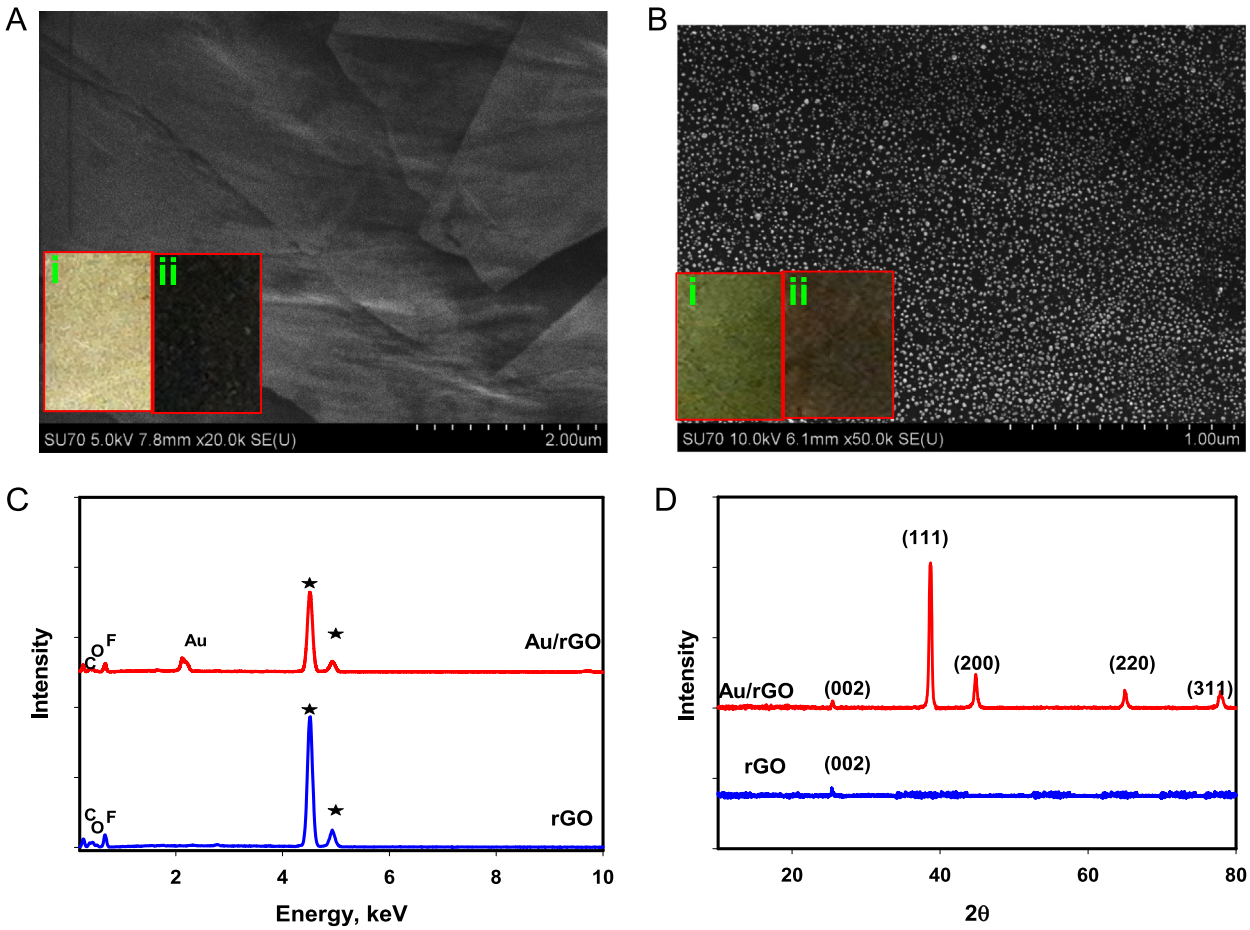

Fig. 1. FE-SEM images obtained for rGO (A) and Au nanoparticle/rGO (B). Inset: Photographs of rGO (A) and Au nanoparticle/rGO (B) films on Ti substrate. (C) EDX spectra of rGO (blue) and Au nanoparticle/rGO (red) films. The peaks marked with asterisks are derived from the Ti substrate. (D) XRD spectra recorded for rGO (blue) and Au nanoparticle/rGO (red). (For interpretation of the references to color in this figure legend, the reader is referred to the web version of this article.)

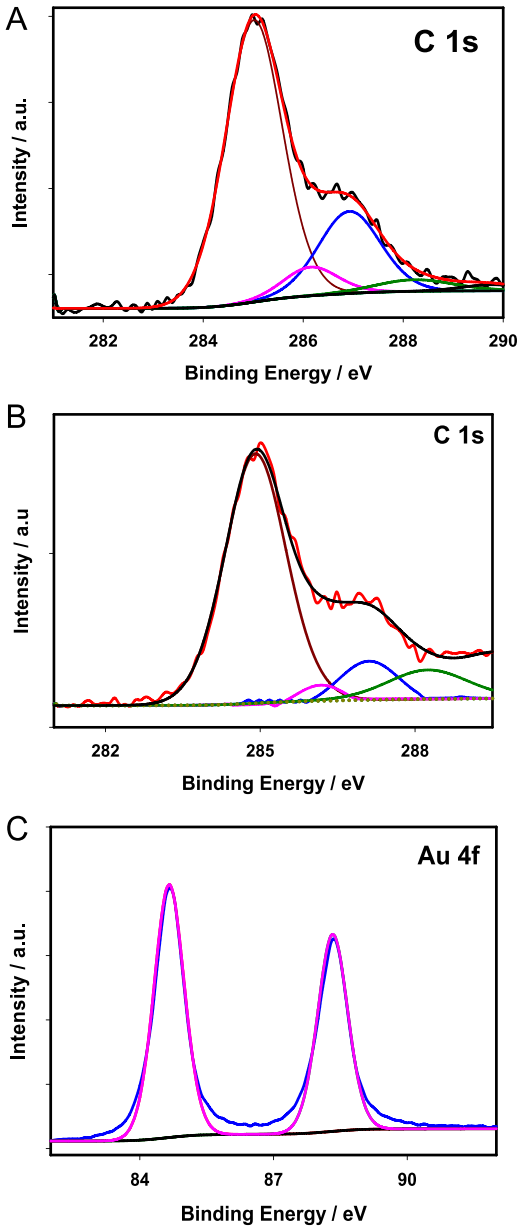

Fig. 2. XPS spectra of the C 1s region for GO (A) and rGO (B); and Au 4f (C) region for the Au-rGO nanocomposite.

reduction peaks, the peak intensities for the Au–rGO/GCE were much higher than that for the Au/GCE. To estimate their electrochemical active surface areas (EASAs), the reduction peaks were integrated to be 188.0 and 344.8 μC for the Au/GCE and Au–rGO/GCE, respectively, revealing that the EASA of the Au–GO/GCE is 1.83 times larger than that of the Au/GCE. It is known that the theoretical charge associated with the reduction of the oxide layer per unit surface area of gold is 400.0 μC cm^{-2} (Oesch and Janata, 1983). The EASAs were calculated to be 0.86 and 0.47 cm^2 for the Au–rGO/GCE and Au/GCE, respectively, which are 12.3 times and 6.7 times higher than the geometric surface area of the GCE substrate.

3.2. Electrochemical oxidation of NADH at the Au nanoparticle/rGO GCE

Fig. 3B compares the cyclic voltammograms (CVs) of the bare GCE (black), rGO/GCE (blue), Au/GCE (pink) and Au–rGO/GCE (red) recorded in 0.1 M PBS (pH 7.2) containing 1 mM NADH at a scan rate of 20 mV s^{-1}. A very small anodic peak was obtained at ~0.7 V for NADH at the bare GCE. For the rGO/GCE, a broad anodic peak appeared at ~0.54 V; whereas a well-defined oxidation peak was observed at 0.63 V for the Au/GCE. Interestingly, a large anodic oxidation peak appeared at the Au–rGO/GCE, with an increase of the current density by ~2.3 times and a negative peak potential shift by ~110 mV in comparison with the Au/GCE. The increased peak current with a negative shift in the NADH oxidation potential reflects a faster electron transfer reaction at the Au–rGO/GCE, showing the capability to efficiently catalyze the electrocatalytic oxidation of NADH. Both the peak potential and current density were stable over the repetitive cycles. To quantitatively analyze the electron transfer of the electrochemical oxidation of NADH, the standard heterogeneous rate constants (k_s) at the rGO/GCE, Au/GCE and Au–rGO/GCE electrodes were calculated using the following equation (Maiyalagan et al., 2013; Velasco, 1997):

$$k_s = 1.11 D_o^{1/2} \left(E_p - E_{p/2}\right)^{-1/2} \upsilon^{1/2}$$

where D_o is the diffusion coefficient; E_p is the oxidation peak potential; $E_{p/2}$ is the half-wave oxidation peak potential and υ is the scan rate. The calculated k_s values were found to be 1.24×10^{-4}, 4.35×10^{-4} and 17.61×10^{-4} cm s^{-1} for the oxidation of NADH at the rGO/GCE, Au/GCE and Au–rGO/GCE electrodes, respectively, revealing that the electron transfer for NADH oxidation at the Au–rGO/GCE electrode was much faster than that at the rGO/GCE and Au/GCE electrodes. Fig. S1 depicts the electrochemical oxidation of NADH to form NAD^+, where two electrons and a proton are involved. The enhanced catalytic activity of the Au–rGO/GCE was facilitated by the highly dispersed Au nanoparticles on the rGO sheets via the formation of a three dimensional electronic conductive network, which was enabled by the intimate contact between the Au nanoparticles and rGO. All the aforementioned results how that the Au nanoparticle/rGO nanocomposite provided an improved electron transfer path and played an important role in the acceleration of electron transfer between the electrode and the NADH.

Fig. 3C presents CVs recorded during the electrocatalytic oxidation of NADH at the Au–rGO/GCEs prepared with different applied timelines for the electrochemical reduction and the formation of Au nanoparticles and rGO nanocomposites varied from 125 to 750 s. As seen in Fig. 3D, increasing the electrochemical reduction time from 125 to 500 s, the peak current was increased; however, further increasing the reduction time from 500 to 750 s, the peak current was decreased and the peak potential slightly shifted to more positive, showing that the optimized electrochemical reduction time was 500 s for the simultaneous formation of the Au nanoparticle and rGO. The effect of the scan rates on the electrochemical oxidation of NADH at the Au–rGO/GCE was also investigated with the CVs presented in Fig. S2A. A linear relationship between the anodic peak current density and the square roote of the scan rate was observed in Fig. S2B, indicating that the electrochemical oxidation of NADH was controlled by the diffusion of electroactive species (Hajian et al., 2014). The anodic peak potential was shifted slightly to the positive with the increase of the scan rates and no reduction peak was observed, showing that the electrochemical oxidation of NADH is irreversible.

3.3. Amperometric sensing of NADH

Fig. S3A depicts amperometric *i–t* curves of the Au–rGO/GCE to investigate the effect of applied potentials on the oxidation of NADH. As seen in Fig. S3B, The steady-state current density was increased with the increase of the applied electrode potential from 0.30 to 0.55 V. However, further increasing the electrode potential

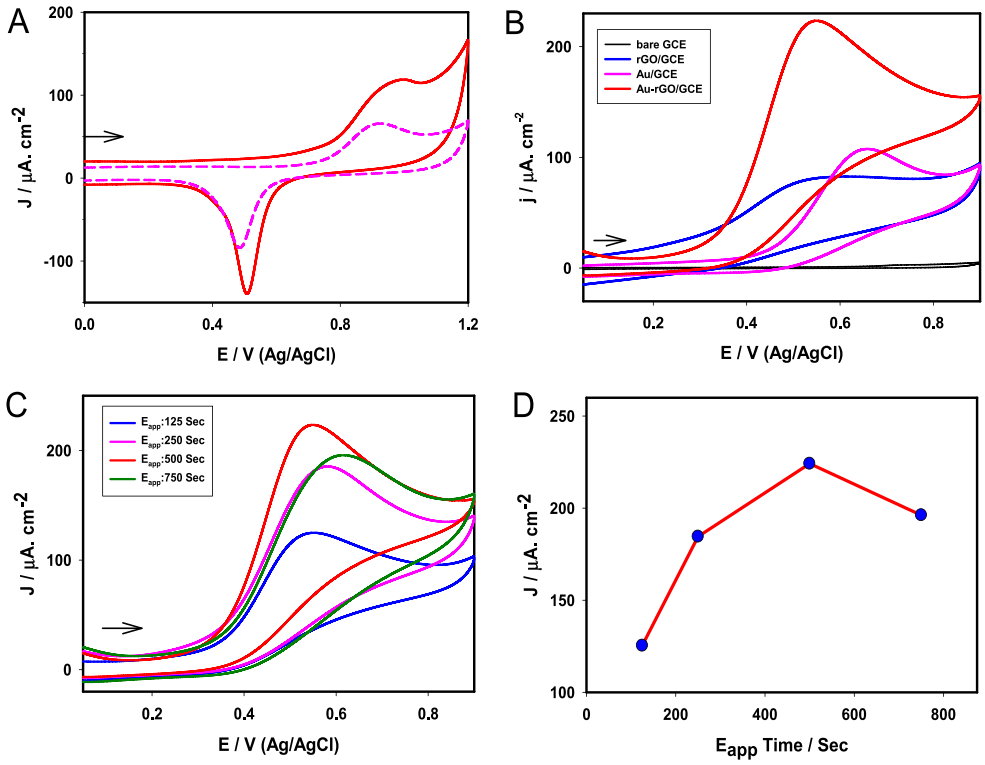

Fig. 3. (A) CVs of the Au/GCE (pink, dashed line) and Au–rGO/GCE (red, solid line) recorded in 0.1 M H_2SO_4. (B) CVs of the GCE (black), rGO/GCE (blue), Au/GCE (pink) and Au–rGO/GCE (red) recorded in 1 mM NADH+0.1 M PBS (pH: 7.2). (C) CVs of the Au–rGO/GCEs, which were prepared at different E_{app} times: 125 (blue), 250 (pink), 500 (red) and 750 s (green), recorded in 1 mM NADH+0.1 M PBS (pH:7.2). Scan rate: 20 mV s^{-1}. (D) The correlation plot of current density against applied time, which was derived from (C). (For interpretation of the references to color in this figure legend, the reader is referred to the web version of this article.)

from 0.55 to 0.60 V, the catalytic current density was slightly decreased, showing that 0.55 V was the optimized potential for the electrochemical oxidation of NADH. This is consistent with the peak potential observed during the electrochemical oxidation of NADH at the Au–rGO/GCE presented in Fig. 3B and Fig. S3A. Fig. 4A displays the amperometric *i*–*t* curve responses for the detection of NADH at the Au–rGO/GCE at the applied potential of 0.55 V. The steady-state current response was attained within three seconds following each addition of NADH. As seen in the inset of Fig. 4A, the experimental detection limit of NADH was below 50 nM. The calibration plots are presented in Fig. 4B, showing two linear concentration ranges: one from 50 nM to 50 μM with a correlation coefficient of $R^2=0.987$ and sensitivity of 0.916 μA/μM cm^2, and the other from 50 μM to 500 μM with a correlation coefficient of $R^2=0.997$ and sensitivity of 0.190 μA/μM cm^2. The limit of detection was calculated to be 1.13 nM using $3\sigma/b$, where σ is the standard deviation of the blank and b is the slope of the calibration curve. Such a low detection limit was far improved from those of most existing reports under similar experimental conditions (Table 1). The electrochemical sensor developed in the present study enabled high sensitivity and a wide linear range, with a low detection limit toward NADH, as shown in Table 1.

3.4. Selectivity, reproducibility and stability of the sensor

Interference from extraneous electroactive compounds could be a challenge in the development of the high-performance electrochemical sensor and biosensor. An assessment of the effects of interference on the amperometric response to NADH was performed at the Au–rGO/GCE in the presence of typical interferents that encompassed glutathione (b), glucose (c), ascorbic acid (d) and gunosine (e) at the applied potential of 0.55 V. Fig. 5A presents the amperometric responses that were obtained at the Au–rGO/GCE with the addition of various interferents. The relative responses to NADH in the absence and in the presence of the interferents as well as to the interferents are presented in Fig. 5B, confirming that the affection of the interferents was almost negligible and that the proposed Au–rGO/GCE possessed a highly selective response to NADH without the use of any selective reagents or enzymes.

The reproducibility of the Au–rGO/GCE was also investigated via the preparation of five different Au nanoparticle/rGO nanocomposite electrodes. The reproducibility tests were carried out in 0.1 M PBS containing 50 μM NADH under the identical experimental conditions. The resulting relative standard deviation (RSD) was found to be 3.64%, which suggested an acceptable reproducibility of the sensor for the detection of NADH. The stability of the Au–rGO/GCE was tested via an amperometric technique in the presence of 1 mM NADH at an applied potential of 0.55 V over 1000 s, where it was observed that the relative current density was decreased less than 9%, as presented in Fig. 5C, suggesting that the fabricated Au–rGO/GCE possessed reasonable good stability toward the electrocatalytic oxidation of NADH. The decrease of the current density can be attributed to the electrode fouling as dimers might be formed during the electrochmeical oxidation of NADH (Moiroux and Elving, 1980; Banks and Compton, 2005). The formed dimers may adsorb on the electrode surface, hindering the heterogeneous charge transfer and resulting in the decrease of the electrocatalytic activity.

3.5. Real sample analysis in human urine

The designed Au–rGO/GCE was further tested to demonstrate its capability for the determination of NADH in real urine samples using the standard addition method. The preparation of the real samples was described in details in the experimental section with

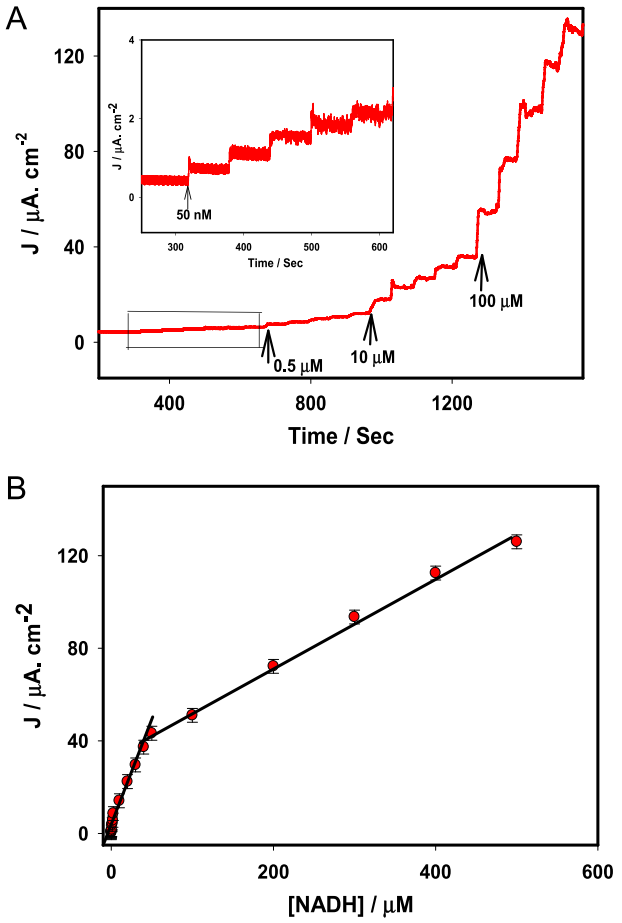

Fig. 4. (A) Amperometric *i–t* curve recorded for the Au–rGO/GCE in 0.1 M PBS under various NADH concentrations (50 nM–0.5 mM), E_{app}:0.55 V. (B) The corresponding calibration plot of current density against NADH concentrations.

the recovery testing results presented in Table S2. High recoveries of NADH between 94.5% and 97.3% with the relative standard deviation (RSD%) values in the range of from 2.6 to 4.3 were achieved, showing the Au nanoparticle/rGO nanocomposites simultaneously formed by in situ electrochemical reduction have strong potential to facilitate applications in biomedical analysis.

4. Conclusions

In this study, we have successfully demonstrated a facile, rapid, cost-effective and green chemistry approach for the in-situ formation of Au nanoparticle/rGO nanocomposites via one-step electrochemical reduction of Au^{3+} and GO. The designed Au nanoparticle/rGO electrode offered much improved and stable

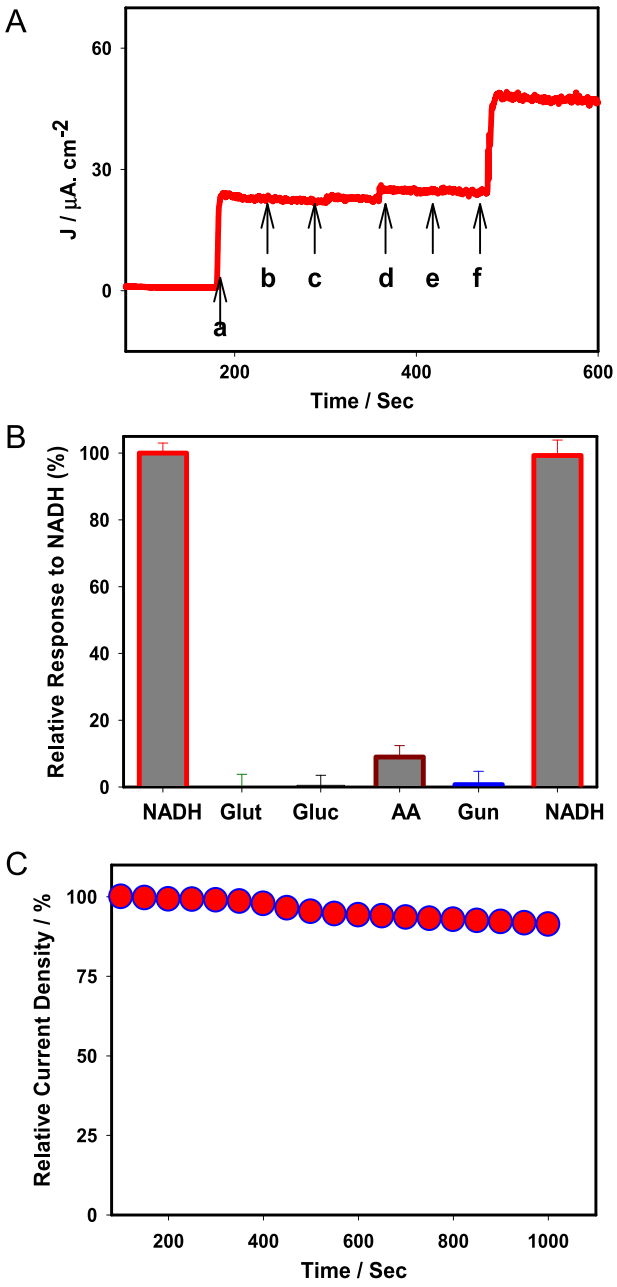

Fig. 5. (A) Amperometric *i–t* curve recorded for the Au–rGO/GCE in 0.1 M PBS with the addition of 50 μM NADH (a), 1 mM of glutathione (b), glucose (c), ascorbic acid (d), gunosine (e) and 50 μM NADH (f) at E_{app}:0.55 V. (B) Comparison of the sensor response in the presence of potential interferents. (C) Amperometric responses obtained for the Au–rGO/GCE in 0.1 M PBS with the addition of 1 mM NADH (E_{app}:0.55 V).

Table 1
Comparison of the recent analytical performance of various electrodes in electrochemical sensing of NADH.

Electrode	Analytical method	LOD (μM)	Sensitivity (μA/μM cm^2)	Linear range	Reference
NiO nanoparticle	Amperometry	0.106	0.052	11 μM–1 mM	Sharifi et al. (2013)
Mesoporous carbon nitride	Amperometry	0.82	0.013	2 μM–2.2 mM	Zhang et al. (2014)
Co_3O_4 nanosheet	Amperometry	4.25	0.027	10–100 μM	Chen et al. (2013)
N_2-diamond nanowire	Differential pulse voltammetry	0.3	0.026	0.5 μM–0.5 mM	Shalini et al. (2014)
NiO	Amperometry	4	0.011	5 μM–0.5 mM	Aydoğdu et al. (2013)
Au nanoparticle/PVC composites	Amperometry	0.05	–	10 μM–10 mM	Garcia-Pineda et al. (2013)
Graphene–Au nanorod	Amperometry	1.5	0.01	5–377 μM	Li et al. (2013)
Au–TiO_2/graphene	Amperometry	0.2	0.02	10–240 μM	Fan et al. (2012)
Au nanoparticle/rGO	**Amperometry**	**0.0011**	**0.916**	**50 nM–0.5 mM**	**This work**

electrocatalytic activity toward the oxidation of NADH without the addition of special reagents or enzymes. The present sensor exhibited high sensitivity with a very low detection limit, wide linear range, good reproducibility and high stability. It also possessed some other advantages, such as ease of fabrication, enhanced electrocatalysis, and effective discrimination from common interfering biomolecules with rapid and stable response to NADH. Additionally, the Au nanoparticle/rGO electrode exhibited a robust capacity for anti-interference with good recovery in human urine samples. To summarize, the novel approach described in this study not only provides an excellent and facile platform for the detection of NADH, but also opens the door for the design of various metal nanoparticles/rGO nanocomposites for promising sensing, energy and environmental applications.

Acknowledgement

This work was supported by a discovery grant from the Natural Sciences and Engineering Research Council of Canada (NSERC). A. Chen acknowledges NSERC and the Canada Foundation for Innovation (CFI) for the Canada Research Chair Award in Materials and Environmental Chemistry.

Appendix A. Supplementary material

Supplementary data associated with this article can be found in the online version at http://dx.doi.org/10.1016/j.bios.2014.12.012.

References

Ali, I., Khan, T., Omanovic, S., 2014. J. Mol. Catal. A: Chem. 387, 86–91.
Ali, I., Omanovic, S., 2014. J. Solid State Electrochem. 18, 833–842.
Artiles, M.S., Rout, C.S., Fisher, T.S., 2011. Adv. Drug Deliv. Rev. 63, 1352–1360.
Aydog˘du, G., Zeybek, D.K., Zeybek, B., Pekyardımcı, S., 2013. J. App. Electrochem. 43, 523–531.
Banks, C.E., Compton, R.G., 2005. Analyst 130, 1232–1239.
Bergel, J.S., Comtat, M., 1989. Anal. Biochem. 179, 382–388.
Bolotin, K.I., 2014. Graphene 4, 199–227.
Chatterjee, S., Wen, J., Chen, A., 2013. Biosens. Bioelectron. 42, 349–354.
Chen, A., Chatterjee, S., 2013. Chem. Soc. Rev. 42, 5425–5543.
Chen, A., Shah, B., 2013. Anal. Methods 5, 2158–2173.
Chen, C.-H., Chen, Y.-C., Lin, M.-S., 2013. Biosens. Bioelectron. 42, 379–384.
Chen, D., Feng, H., Li, J., 2012. Chem. Rev. 112, 6027–6053.
Chikkaveeraiah, B.V., Bhirde, A.A., Morgan, N.Y., Eden, H.S., Chen, X., 2012. ACS Nano 6, 6546–6561.
Cullity, B.D., 1978. Elements of X-ray Diffraction. Addision-Wesley, Reading, MA. p. 102.
Dalkiran, B., Kaçar, C., Erden, P.E., Kiliç, E., 2014. Sens. Actuators B: Chem. 200, 83–91.
Deore, B.A., Freund, M.S., 2005. Chem. Mater. 17, 2918–2923.
Downey, T.M., Nieman, T.A., 1992. Anal. Chem. 64 (261-268).
Fan, Y., Yang, X., Yang, C., Liu, J., 2012. Electroanalysis 24, 1334–1339.
Garcia-Pineda, I., Mayen, M., Rodriguez-Mellado, J.M., Rodriguez-Amaro, R., 2013. Electroanalysis 25, 1981–1987.
Govindhan, M., Chen, A., 2015. J. Power Sour. 274, 928–936.
Hajian, R., Yusof, N.A., Faragi, T., Shams, N., 2014. PLOS One 9, 1–7.
Kimmel, D.W., LeBlanc, G., Meschievitz, M.E., Cliffel, D.E., 2012. Anal. Chem. 84, 685–707.
Li, H., Li, R., Worden, R.M., Barton, S.C., 2014. ACS Appl. Mater. Interfaces 6, 6687–6696.
Li, L., Lu, H., Deng, L., 2013. Talanta 113, 1–6.
Limoges, B., Marchal, D., Mavre, F., Saveant, J., 2006. J. Am. Chem. Soc. 128, 2084–2092.
Lin, K.C., Lai, S.Y., Chen, S.M., 2014. Analyst 139, 3991–3998.
Lin, S.-J., Guarente, L., 2003. Curr. Opin. Cell Biol. 15, 241–246.
Lin, W., Xueji, Z., Huangxian, J., 2007. Anal. Chem. 79, 453–458.
Liu, C., Jiang, D., Xiang, G., Liu, L., Liu, F., Pu, X., 2014. Analyst 139, 5460–5465.
Liu, F., Xiang, G., Yuan, R., Chen, X., Luo, F., Jiang, D., Huang, S., Li, Y., Pu, X., 2014. Biosens. Bioelectron. 60, 210–217.
Liu, M., Chen, Q., Lai, C., Zhang, Y., Deng, J., Li, H., Yao, S., 2013. Biosens. Bioelectron. 48, 75–81.
Liu, S., Du, Z., Li, P., Li, F., 2012. Biosens. Bioelectron. 35, 443–446.
Luo, Z., Yuan, X., Yu, Y., Zhang, Q., Leong, D.T., Lee, J.Y., Xie, J.J., 2012. J. Am. Chem. Soc. 134, 16662–16670.
Maduraiveeran, G., Ramaraj, R., 2007. J. Electroanal. Chem. 608, 52–58.
Maiyalagan, T., Sundaramurthy, J., Kumar, P.S., Kannan, P., Opallo, M., Ramakrishna, S., 2013. Analyst 138, 1779–1786.
Moiroux, J., Elving, P.J., 1980. J. Am. Chem. Soc. 102, 6533–6538.
Moradi, R., Sebt, S.A., Karimi-Maleh, H., Sadeghi, R., Karimi, F., Baharie, A., Arabif, H., 2013. Phys. Chem. Chem. Phys. 15, 5888–5897.
Oesch, U., Janata, J., 1983. Electrochim. Acta 28, 1247–1253.
Pelaz, B., Pino, P., 2012. Synthesis applications of gold nanoparticles. Front. Nanosci. 4, 3–33 (chapter 1).
Qian, Y., Lu, S., Gao, F., 2011a. J. Mater. Sci. 46, 3517–3522.
Qian, Y., Lu, S., Gao, F., 2011b. Mater. Lett. 65, 56–58.
Radoi, A., Compagnone, D., 2009. Bioelectrochemistry 76, 126–134.
Ricci, F., Amine, A., Moscone, D., Palleschi, G., 2007. Biosens. Bioelectron. 22, 854–862.
Saha, K., Agasti, S.S., Kim, C., Li, X., Rotello, V.M., 2012. Chem. Rev. 112, 2739–2779.
Serban, S., Murr, N.E., 2004. Biosens. Bioelectron. 20, 161–166.
Shalini, J., Sankaran, K.J., Chen, H.-C., Lee, C.-Y., Tai, N.-H., Lin, I.-N., 2014. Analyst 139, 778–785.
Sharifi, E., Salimi, A., Shams, E., 2013. Biosens. Bioelectron. 45, 260–266.
Turner, A.P.F., 1988. Methods Enzymol. 137, 90–103.
Vedala, H., Sorescu, D.C., Kotchey, G.P., Star, A., 2011. Nano Lett. 11, 2342–2347.
Velasco, J.G., 1997. Electroanalysis 9, 880–882.
Wagner, C.D., Riggs, W.M., Davis, L.E., Moulder, J.F., Muilenberg, G.E., 1979. Handbook of X-ray Photelectron Spectroscopy. Perkin-Elmer Corporation, Minnesota, USA, p. 38.
Wang, G.-L., Xu, J.-J., Chen, H.-Y., 2009. Biosens. Bioelectron. 24, 2494–2498.
Wang, J., Thomas, D.F., Chen, A., 2008. Anal. Chem. 80, 997–1004.
Wei, H.Z., van de Ven, T.G.M., Omanovic, S., Zeng, Y.W., 2008. Langmuir 24, 12375–12384.
Wu., L., Zhang, X., Ju, H., 2007. Anal. Chem. 79, 453–458.
Xu, Z., Gao, C., 2011. Nat. Commun. 571, 1–9.
Zhang, Y., Bo, X., Nsabimana, A., Luhana, C., Wang, G., Wang, H., Li, M., Guo, L., 2014. Biosens. Bioelectron. 53, 250–256.